Submitted 15 Sept 1948
Optics Letters

Broadband monolithic acousto-optic tunable filter

H. Gnewuch, N. K. Zayer, C. N. Pannell

University of Kent at Canterbury, School of Physical Sciences, Canterbury CT2 7NZ, United Kingdom

G. W. Ross, P. G. R. Smith

University of Southampton, Optoelectronics Research Centre, Southampton SO17 1BJ, United Kingdom

Abstract

Broadband monolithic acousto-optic tunable filters (MAOTFs) combining piezoelectric transducer array and acousto-optic interaction medium in a single crystal have been investigated. A linearly chirped acoustic superlattice with an optical tuning range between $\lambda = 1.3$ and 1.6 μm was formed by domain inversion in $LiNbO_3$. X-propagating longitudinal acoustic waves are excited in "crossed-field" scheme by an RF E_y-field applied to the superlattice and couple collinearly propagating e- and o-polarised optical modes. At $\lambda = 1.319$ μm and 1.55 μm, the spectral bandwidth (FWHM) were 1.54 and 2.3 nm respectively. A relative conversion efficiency of 43 %/W, and a maximum conversion efficiency of 51 %, were measured at 1.319 μm.

Acousto-optic tunable filters (AOTFs) are attractive components due to their potential wide tuning range and narrow filter bandwidth and thus find many applications such as in optical networks[1] and tunable lasers[2]. The performance of bulk AOTFs has been steadily improved[3] since their invention[4] but the basic design consisting of separate crystals for acoustic transducer and acousto-optic interaction medium is unaltered. The necessary fabrication processes such as crystal bonding and transducer lapping/polishing are labour-intensive and thus costly. Furthermore, the electrodes and bond layers are part of the sound transmission path and affect its spectral transmission properties[5].

Recently, acoustic transducer arrays, also called acoustic superlattices (ASLs), have been formed by domain inversion in ferroelectric crystals using various techniques, and their acoustic properties have been studied and derived for a variety of configurations[6–9]. ASLs may be subdivided into an "in-line" and "crossed-field" scheme[10] indicating an applied electric field to be parallel or perpendicular to the propagation direction of the excited acoustic wave, respectively. By using ASLs, transducer and interaction medium can be combined into a contiguous piece of $LiNbO_3$ and by exciting acoustic waves in a crossed-field scheme the soundpath is not obstructed by bonds or electrodes, thus overcoming the aforementioned problems.

In this Letter we present the first optical measurements on an MAOTF in which the ASL is formed within part of the acousto-optic interaction medium, resulting in a more compact device of greatly simplified construction. We discuss briefly how domain inversion in $LiNbO_3$ influences the physical effects relevant to the operation of the device.

Superlattices in $LiNbO_3$ have the spontaneous polarization either parallel, Fig. 1(a), or perpendicular, Fig. 1(b), to the domain walls, depending on the fabrication process[6,7]. The crystal unit cells of domains with antiparallel spontaneous polarizations are, of course, congruent and can be transformed into each other by a 180° rotation about the x-axis (perpendicular to a symmetry plane). Thus, upon inversion the y and z axis change sign which results in change of sign for all odd ranked tensor elements, e.g. piezoelectric coefficients e_{Ik} Fig. 1(d), whereas all even ranked tensor elements remain unchanged, see Fig. 1(c)

where ε_{ij}, c_{IJ}, and p_{IJ} are the permittivity, elastic stiffness, and photoelastic coefficients, respectively. Here we consider an x-propagating longitudinal acoustic wave excited by a "crossed" i.e. y-directed time-harmonic electric field E_2. The resulting displacement field u_1 is described by a driven 1-D Helmholtz equation Eq.(1),

$$\frac{\partial^2 u_1(x)}{\partial x^2} + k_a^2 u_1(x) = -\frac{\partial e_{22}(x)}{\partial x}\frac{E_2}{c_{11}} \tag{1}$$

where $k_a = 2\pi f_a / v_{l,1}$ is the wavenumber of the wave having frequency f_a and phase velocity $v_{l,1}$. Note that the source term contains the derivative of e_{22} Fig. 1(e). Thus, the domain boundaries of the ASL can be viewed as alternating δ-function sources of the acoustic field. By choosing suitable dimensions for the ASL and varying its period Λ, as indicated in Fig. 1, the transducer can be made efficient over a broad band.

In order to demonstrate such tunability we fabricated a device from a z-cut $LiNbO_3$ wafer of thickness $W = 500$ μm which was patterned with a linearly chirped grating having periods between $\Lambda_1 = 17.25$ μm and $\Lambda_2 = 22.0$ μm over a length $L_g = 10$ mm, Fig. 2(a). The sample was then poled[11] and sawn parallel to the x-axis. After polishing the ends at an angle $\alpha = 10$ ° to the x-faces, resulting in $L = 20$ mm and $d = 0.67$ mm, chrome-gold electrodes were deposited onto the y-faces over a length $L_e = 14$ mm, covering the ASL, Fig. 2(b). One electrode was indium bonded to the outer conductor of a 50 Ω coplanar waveguide stripline whereas the other electrode was bonded with gold wires to the center conductor. Here, the indium bonded electrode functions also as an absorber of acoustic waves backreflecting at the wedged ends into the sample under an oblique angle to the x-axis.

The frequency dependent excitation (and detection) of the bulk acoustic waves in the device was determined by measuring the electrical reflection coefficient with a network analyzer. Figure 3(a) shows $|S_{11}|^2$, equivalent to the ratio of reflected to incident electrical power P_r/P_i, as a function of frequency. Ignoring dissipative losses the $\sim$ -3 dB change over the passband corresponds to $\sim$ 50 % of P_i converted into acoustic power P_a. The ASL passband was designed to extend from $f_2 = v_{l,1}/\Lambda_2 = 298.6$ MHz, and $f_1 = v_{l,1}/\Lambda_1 = 380.9$ MHz.

As the poling process leaves the photoelastic coefficients unaltered the mode conversion follows standard coupled mode theory. The power conversion efficiency between the orthogonally polarised e and o modes is $\eta = P_{e,o}(L_i)/P_{o,e}(0) = (\kappa L_i)^2 \mathrm{sinc}^2(\sqrt{\kappa^2 + \delta^2} L_i)$ where L_i, κ, and δ denote interaction length, coupling coefficient, and phasemismatch, respectively. Maximum coupling requires the polarization modes with a birefringence $\Delta\beta = |\beta_e - \beta_o|$ to be phasematched by the acoustic wave having a wavenumber $K = 2\pi/\lambda_{a,0}$, i.e. $2\delta = 0 = \Delta\beta - K$. η varies rapidly by changing the optical wavelength λ (acoustic frequency f_a) for a fixed $f_{a.0}$ (λ_0) at $\delta = 0$ which is described by the normalized filter bandwidth (FWHM)

$$\left.\frac{\Delta f_a}{f_{a,0}}\right|_{\lambda_0} = \left.\frac{\Delta\lambda}{\lambda_0}\right|_{f_{a,0}} = 0.797 \left.\frac{\lambda_a}{L_i}\right|_{(a)} = 0.885 \left.\frac{\lambda_a}{L_i}\right|_{(b)}. \tag{2}$$

Here, the subscripts (a) and (b) denote a maximum conversion of $\eta_{max} = 1$ ($\kappa L_i = \pi/2$) and $\eta_{max} < 0.1$ ($\kappa L_i < \pi/10$), respectively. At $\delta = 0$, η becomes

$$\eta = \sin^2\left[\frac{\pi L_i}{\lambda_0}\sqrt{\frac{M_2}{2}\frac{P_a}{A_a}}\right] \tag{3}$$

where $M_2 = (n_e n_o/v_{l,1})^3 p_{41}^2/\rho$, P_a, and A_a are the figure of merit, acoustic power, and the acoustic wave cross-section, with ρ as density and p_{41} as the relevant off-diagonal elastooptic coefficient.

In order to demonstrate acousto-optic operation over the whole passband, light sources LS, Fig. 2(c), were used at extreme ends of the spectrum. In both cases the light from LS was passed through a single mode fiber, a microscope objective transforming it into a circular beam with a confocal parameter $b \sim 70$ mm, and an e-oriented polarizer P. The sample was positioned each time with the beam parallel to its x-axis and the beam waist at its center, $x = L/2$. An RF power meter was used to measure the power delivered to the MAOTF.

Firstly, a narrow linewidth Nd:YAG laser operating at $\lambda_0 = 1319$ nm was used. For the determination of the filter characteristic an RF power of $P_i \sim 100$ mW was applied to the device and square wave modulated at $f_{AM} \sim 14$ kHz. The output light from the sample was passed through an o-polarized analyzer A to a GaAs detector PD and its modulated

signal δP_o was measured with a lock-in amplifier, Fig. 2(c), while the RF frequency f_a was adjusted. The reference signal δP_e was obtained by rotating the analyzer to be inline with the polarizer and by using a mechanical chopper (50 % duty cycle) in the lightpath. Figure 3(b) depicts the result with $\eta = \delta P_o/\delta P_e$ normalized by its maximum value of $\sim$ 2 % at the center frequency $f_{a,0}$. With an RF bandwidth of Δf_a = 430 kHz around $f_{a,0}$ = 369.15 MHz and an acoustic wavelength of $\lambda_a = v_{l,1}/f_{a,0}$ = 17.8 μm the FWHM and the interaction length were calculated to $\Delta\lambda$ = 1.54 nm and L_i = 13.5 mm, respectively, Eq.(2). Note that L_i is smaller than L and close to L_e. This may be explained by an increased sample temperature along the electrodes due to the acoustic power being absorbed. As the calculated[12] matching wavelength-temperature gradient $\partial\lambda_0/\partial T = \lambda_a[\partial(\Delta n)/\partial T] \sim$ - 0.55 nm/K only 3 °C will cause the difference between λ_0 within and outside the electroded area to become larger than the measured filter bandwidth.

For the determination of η versus applied acoustic power P_a at that specific wavelength the RF signal was amplitude modulated as before, the analyzer was kept parallel to the polarizer, and the detector signal was monitored with an oscilloscope. This has the advantage of obtaining η directly from the contrast $(P_{off} - P_{on})/P_{off}$ where P_{on} and P_{off} are the detector levels measured with and without applied P_a, respectively. Figure 3(c) shows the measured data at matched phase conditions. A maximum relative conversion efficiency of η_r = 43 %/W was obtained and a conversion efficiency η = 51 % at $P_a \sim$ 2 W was achieved limited by the available drive power. Figure 3(c) also depicts the relation $\eta = \sin^2[(\pi/2)\sqrt{P_a/P_{a,0}}]$, according to Eq.(3), fitted to the data set with an R^2 = 0.996, an estimated acoustic power for full conversion, and photoelastic coefficient of $P_{a,0}$ = (7.74 $\pm$ 0.12) W and $p_{41} \sim$ 0.05, respectively. Note that p_{41} at this wavelength is about a third compared to published data at λ_0 = 0.633 μm[13].

Secondly, a broad band ASE source with a center wavelength at 1550 nm and a bandwidth of 40 nm, crossed polarizers and an optical spectrum analyzer were used. Two examples of filter responses are depicted in Fig. 3(d) where $f_{a,1}$ = 312.10 MHz (solid line), $f_{a,2}$ = 306.56 MHz (dashed line), and $P_a \sim$ 300 mW. A minimum spectral bandwidth of $\Delta\lambda \sim$ 2.3 nm

was measured which requires an L_i of $\sim$ 12.8 mm, Eq.(2). Compared to the results at $\lambda_0 =$ 1319 nm the slightly reduced interaction length may be caused by an increased temperature gradient close to the edges of the electrodes due to increased drive power.

In conclusion, we have demonstrated the operation of a novel monolithic AOTF. The device incorporates transducers which are formed by ferroelectric domain inversion, and the transmission medium in a single $LiNbO_3$ crystal and is thus simpler to build than conventional bulk AOTFs. A chirped transducer array (ASL) provides broadband excitation of longitudinal acoustic waves which couple collinearly propagating optical polarization modes. Both the optical bandwidth and the RF power requirement could be significantly reduced by minimising temperature gradients along the device.

H. Gnewuch acknowledges the financial support by the EPSRC (UK) under the project GR/L05419.

REFERENCES

1. K. W. Cheung, IEEE J. Select. Areas Commun. **SAC-8**, 1015 (1990).

2. G. Coquin and K. W. Cheung, Electron. Lett. **24**, 599 (1988).

3. C. S. Qin, G. C. Huang, K. T. Chan, and K. W. Cheung, Electron. Lett. **31**, 1237 (1995).

4. S. E. Harris, S. T. K. Nieh, and D. K. Winslow, Appl. Phys. Lett. **15**, 325 (1969).

5. E. K. Sittig, IEEE Trans. Sonics and Ultrasonics **SU-16**, 2 (1969).

6. Y. Y. Zhu and N. B. Ming, J. Appl. Phys. **72**, 904 (1992).

7. Y. F. Chen, S. N. Zhu, Y. Y. Zhu, N. B. Ming, B. B. Jin, and R. X. Wu, Appl. Phys. Lett. **70**, 592 (1997).

8. S. D. Cheng, Y. Y. Zhu, Y. L. Lu, and N. B. Ming, Appl. Phys. Lett. **66**, 291 (1995).

9. Y. Y. Zhu, S. N. Zhu, Y. Q. Qin, and N. B. Ming, J. Appl. Phys. **79**, 2221 (1996).

10. W. R. Smith, H. M. Gerard, J. H. Collins, T. M. Reeder, and H. J. Shaw, IEEE Trans. Microwave Theory Tech. **MTT-17**, 856 (1969).

11. J. Webjörn, V. Pruneri, P. St. J. Russell, J. R. M. Barr, and D. C. Hanna, Electron. Lett. **30**, 894 (1994).

12. G. J. Edwards and M. Lawrence, Opt. Quant. Electron. **16**, 373 (1984).

13. R. S. Weis and T. K. Gaylord, Appl. Phys. A **37**, 191 (1985).

FIGURES

Fig. 1. (a,b) Superlattice with spontaneous polarization (a) parallel and (b) perpendicular to domain walls; Viewed along corresponding superlattice : (c) even-ranked tensor elements; (d) piezoelectric tensor elements; (d) spatial derivate of piezoelectric tensor elements understood as acoustic sources.

Fig. 2. (a,b) Schematic of device : (a) Superlattice in $LiNbO_3$ linearly chirped between period Λ_1 and Λ_2 over length L_g, W width, ends wedged at angle α; (b) L overall length, L_e electrode length, d depth; (c) Experimental setup : RF signal excites acoustic causing coupling between e- and o- polarized modes, LS light source, P linear polarizer, A linear analyzer, PD photodiode, η modulation signal.

Fig. 3. (a) Measured squared magnitude of backscatter signal $|S_{11}|^2$ versus acoustic frequency f_a; (b,c) measured conversion efficiency η at $\lambda = 1.319$ μm with respect to (a) acoustic frequency f_a, and (b) acoustic power P_a; (d) measured conversion efficiency η versus wavelength λ for f_{RF} = 312.1 MHz (solid line) and 306.56 MHz (dashed line).

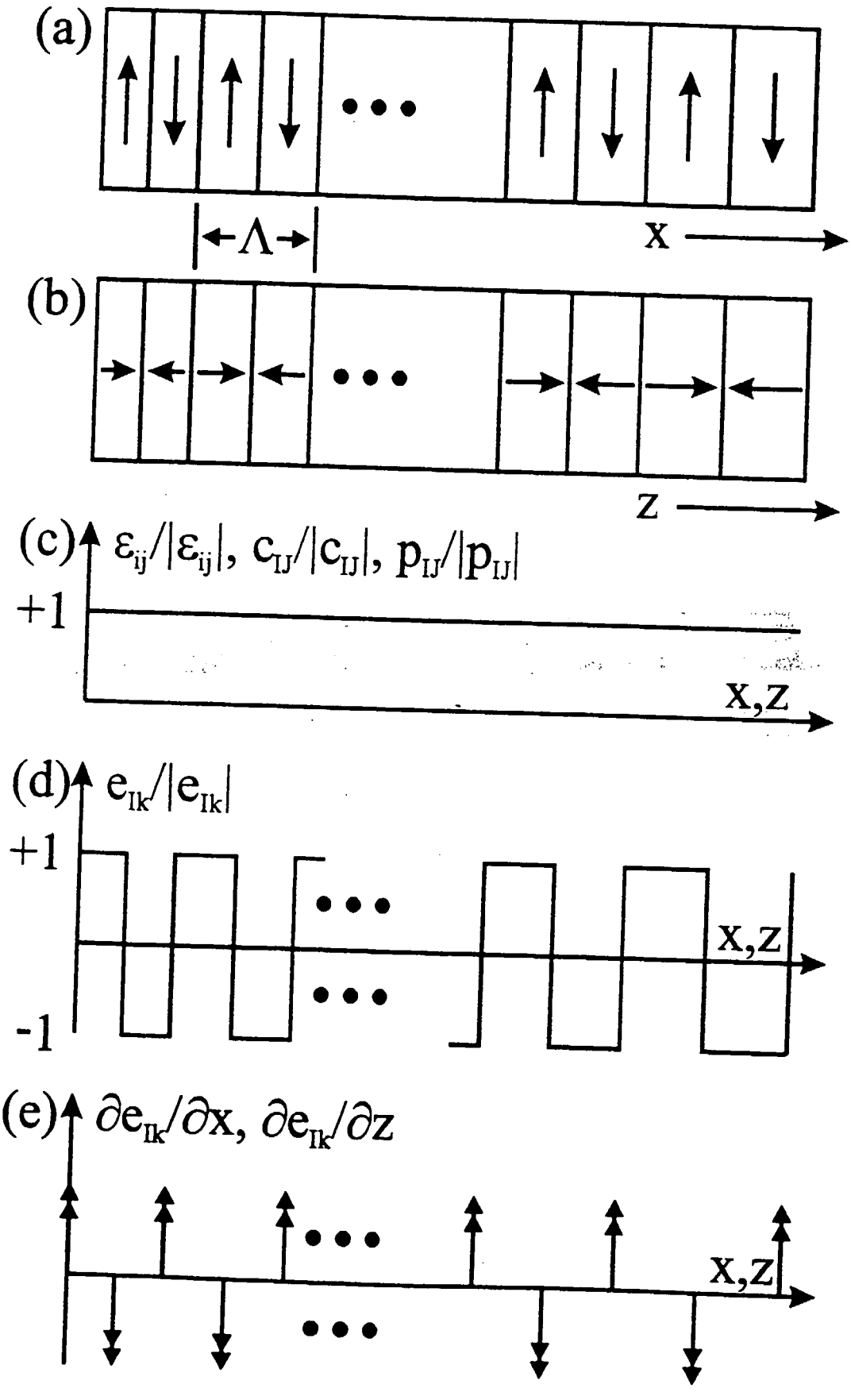

Fig. 1: H.Gnewuch et al : "Broadband monolithic acousto-optic ..."

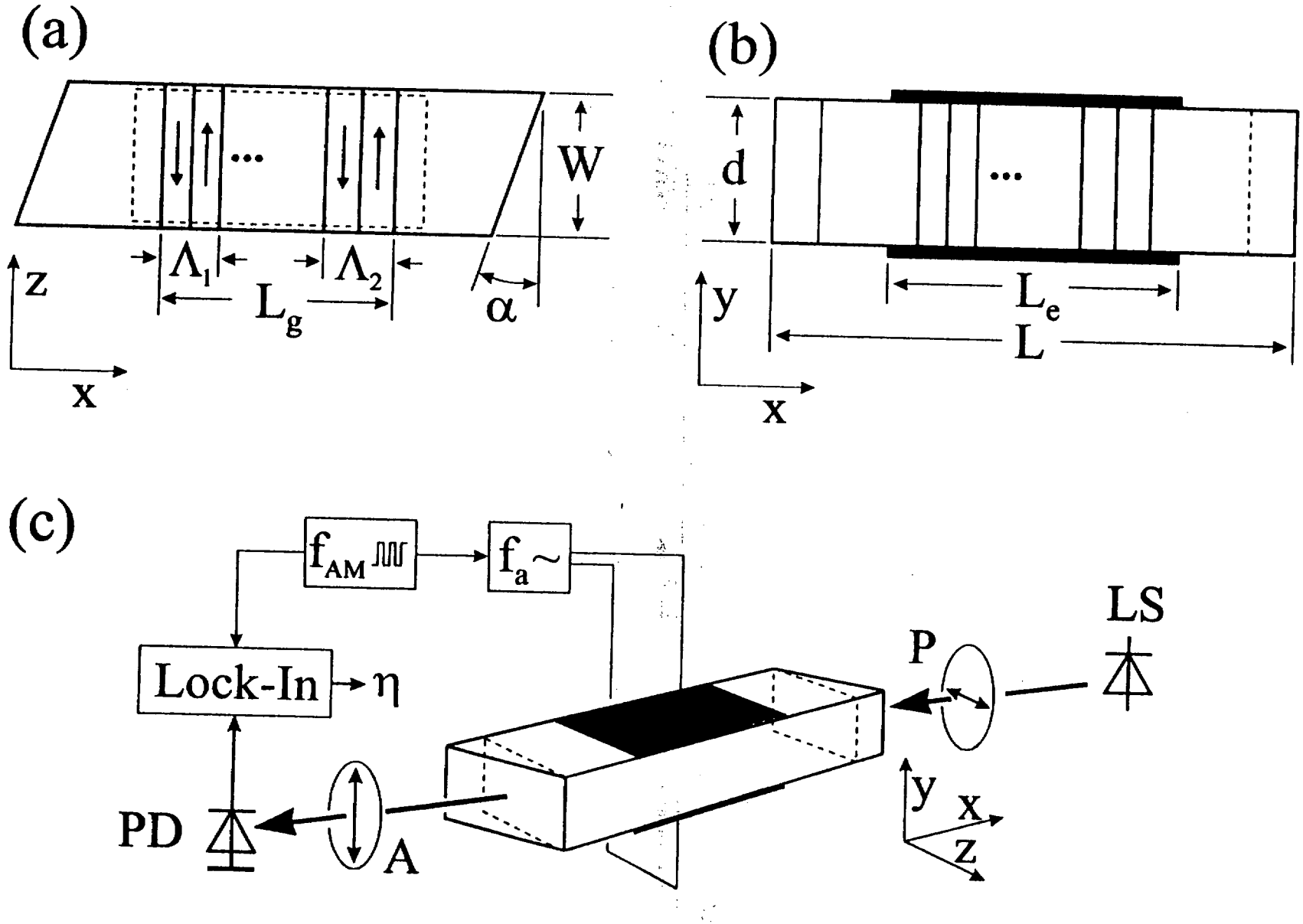

Fig. 2: H. Gnewuch et al : "Broadband monolithic acousto-optic ..."

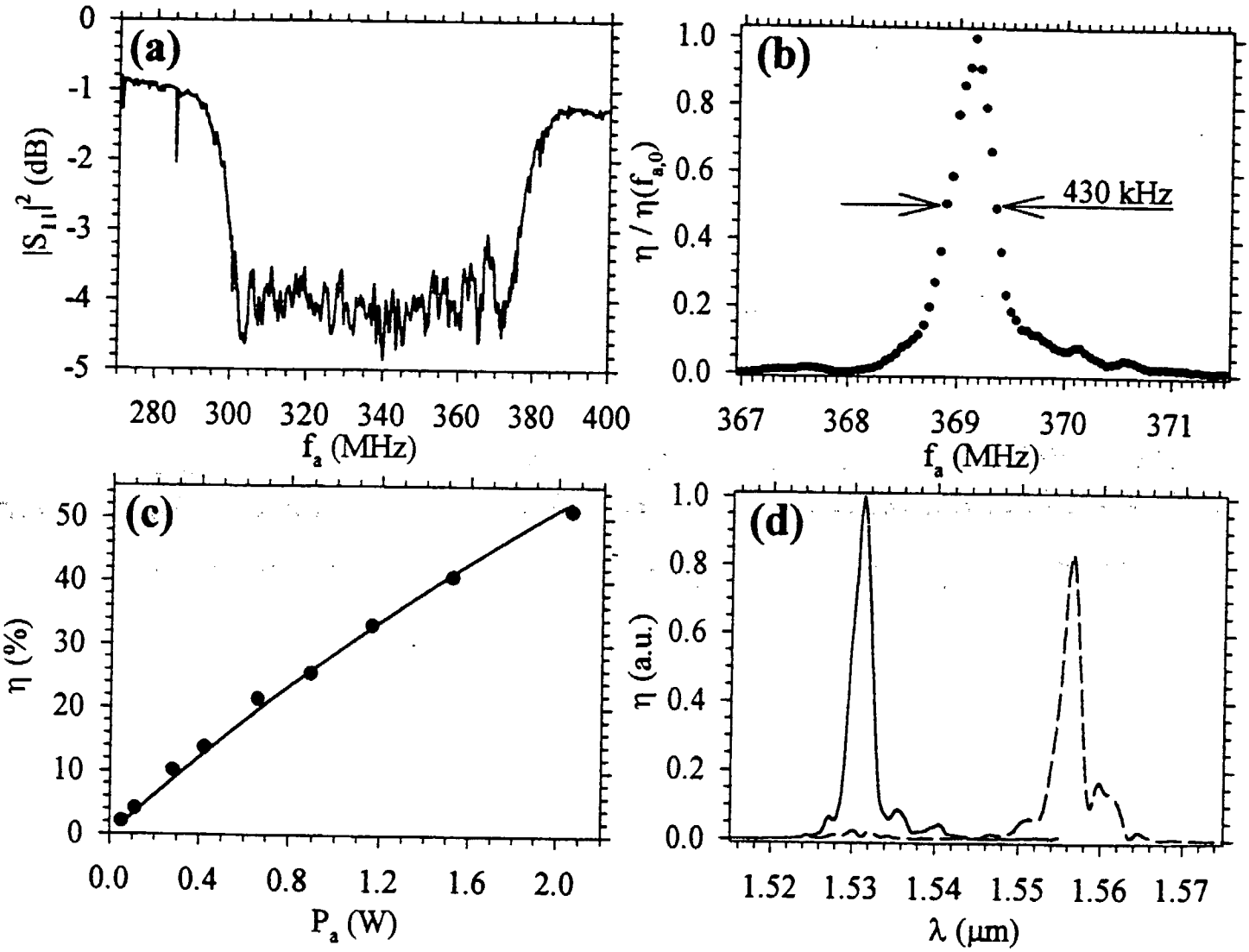

Fig. 3: H. Gnewuch et al : "Broadband monolithic acousto-optic ..."